50th AIAA Aerospace Sciences Meeting including the New Horizons Forum and Aerospace Exposition
09 - 12 January 2012, Nashville, Tennessee

AIAA 2012-0080

Manufactured Solutions for the Favre-Averaged Navier-Stokes Equations with Eddy-Viscosity Turbulence Models

Todd A. Oliver*, Kemelli C. Estacio-Hiroms†, Nicholas Malaya‡, Graham F. Carey§
The University of Texas at Austin, Austin, TX, 78712, USA

The Method of Manufactured Solutions is applied to verify the implementation of eddy viscosity turbulence models for closure of the Favre-averaged Navier-Stokes equations. In the Method of Manufactured Solutions, the governing equations are modified by the addition of source terms such that the exact solution—i.e., the manufactured solution—is known *a priori*. Given the exact solution, order of accuracy studies are conducted to verify that the discrete solution converges to the exact solution at the expected rate. The goal of this work is to verify the implementation of turbulence models in the Fully-Implicit Navier-Stokes flow solver. The turbulence model of interest for this work is the Spalart-Allmaras one-equation model, and two manufactured solutions have been examined. The first solution is based on trigonometric functions, as commonly used in manufactured solution literature. This solution is appropriate for use in unbounded flows, enabling verification of the implementation of the free shear flow form of the model. The second solution has been newly developed in this work and is intended for use in wall-bounded flows. While other manufactured solutions for the Spalart-Allmaras model for wall-bounded flow have appeared in the literature, these solutions are shown to have features that make them ill-suited to verification. To avoid such features, the wall-bounded solution developed here is loosely based on the behavior of the model solution in the inner portion of a zero-pressure boundary layer. Results obtained using both solutions show that the Fully-Implicit Navier-Stokes flow solver is achieving the expected second-order accuracy.

I. Introduction

Numerical simulations are critical in all areas of science and engineering. Simulation results are used both to further understanding of physical phenomena and to inform critical engineering decisions. Given this importance, verification of the software used to perform these simulations has become essential. Verification is the process of ensuring that the software implementation of a mathematical model is correct (code verification) and that discrete solutions obtained using that implementation are sufficiently accurate relative to the exact solution of the model (solution verification).[1–4]

A powerful verification technique is the Method of Manufactured Solutions (MMS). In the MMS, the governing equations are modified by the addition of source terms such that the exact solution—i.e., the manufactured solution—is known *a priori*.[5,6] Given the exact solution, order of accuracy studies are conducted to verify that the discrete solution converges to the exact solution at a rate consistent with the numerical discretization scheme.

The goal of this work is to apply the MMS to verify the implementation of the Spalart-Allmaras (SA) turbulence model[7] in the Fully-Implicit Navier-Stokes (FIN-S) flow solver.[8,9] A number of previous authors have studied manufactured solutions for turbulence models. For example, Roy et al.[10] developed a manufactured solution for Menter's k-ω model and applied it to the Loci-CHEM CFD code. Their solution is a

*Research Associate, Institute for Computational Engineering and Sciences, Member AIAA
†Postdoctoral Researcher, Institute for Computational Engineering and Sciences, Member AIAA
‡Research Engineer, Institute for Computational Engineering and Sciences, Member AIAA
§The authors wish to dedicate this paper to the memory of Professor Graham F. Carey, whose research and teaching have greatly influenced the development of finite element methods, computational mechanics, and supercomputing over the last thirty-five years. Dr. Carey was a mentor, advisor and kind friend to the authors of this paper. He will be greatly missed.

sum of trigonometric functions and does not satisfy the no-slip condition. Bond et al.[11] developed a general methodology for generating manufactured solutions that satisfy a desired boundary condition and applied it to multiple turbulence models, including SA.

While the Bond[11] solutions satisfy no-slip, they are otherwise not physically realistic. Because verification is purely a mathematical exercise, the manufactured solution does not need to be close to any actual solution of the model of interest, and it may not be representative of any actual physical situation. However, as noted by Eça et al.,[12,13] choosing a physically realistic manufactured solution does offer some advantages. Most importantly, for physically realistic solutions, it is expected that each term in the PDE will be exercised in a manner similar to that of a real problem. This feature is important in posing a strong verification test. When the terms of the PDE are not exercised in a physically meaningful way, it is possible to design manufactured solutions where the dominant balance in the equation is controlled by only a subset of the terms of the actual equation, potentially hiding implementation errors. Alternatively, it is also possible to design a manufactured solution that introduces problems, e.g., instabilities, that are not observed for actual model solutions.

These issues are particularly relevant in the case of attached, wall-bounded, turbulent flows. Near the wall, popular engineering models used to simulate such flows have complicated but generally understood behaviors. Thus, these behaviors should be reflected in a physically realistic manufactured solution. Eça and co-authors[12–14] developed solutions for multiple turbulence models that are intended to mimic two-dimensional, incompressible, stationary boundary layer flow. However, they note that generating physically realistic solutions for the near-wall region in turbulent flows is challenging, and they do not observe the expected order of accuracy for two of the manufactured solutions generated for the SA model.[14]

In this work, two manufactured solutions for the Favre-averaged Navier-Stokes (FANS) equations coupled with the SA turbulence model are developed. Like the solutions generated by Roy et al.,[10,15] the first solution is constructed as a sum of sine and cosine functions. This solution does not satisfy the no-slip boundary condition on any boundary and, thus, is only appropriate to test the model implementation far from walls. However, since wall-bounded flows are of significant interest in FIN-S applications, a solution that satisfies the no-slip boundary condition on some portion of the boundary is required. Similar to Eça et al.,[12–14] the solution developed here is intended to be physically realistic. To aid in this construction, the solutions proposed by Eça et al.[14] are analyzed to help understand potential sources of difficulties. Then, in an attempt to avoid pathological behaviors in the solution and required source terms near the no-slip boundary, the new manufactured solution is constructed to loosely resemble the inner portion (viscous sublayer + logarithmic layer) of a zero pressure gradient boundary layer. To accomplish this goal, the manufactured solution is built using well-known correlations for turbulent boundary layers and the expected near-wall behavior of the SA state variable.

These new manufactured solutions have been implemented in the Manufactured Analytical Solution Abstraction (`MASA`) library,[16] an open source software library designed to act as a repository for manufactured solutions. The FANS-SA capabilities in FIN-S have been tested using this library, and the results show that the discrete solutions converge as expected (i.e., the L_2 norm of the error is $\mathcal{O}(h^2)$, where h is the grid spacing) for both manufactured solutions.

II. Mathematical Model

The mathematical model of interest is the FANS equations coupled with the SA turbulence model.[7] While these equations are generally well-known, they are specified here for completeness.

The FANS equations express the mean conservation of mass, momentum, and energy. These mean equations are unclosed due to averaging over nonlinear terms, which necessitates the addition of a turbulence

model to close the system. Using the SA turbulence model, the governing equations are as follows:

$$\frac{\partial \bar{\rho}}{\partial t} + \frac{\partial}{\partial x_i}(\bar{\rho}\tilde{u}_i) = 0,$$

$$\frac{\partial}{\partial t}\left(\bar{\rho}\tilde{u}_i\right) + \frac{\partial}{\partial x_j}\left(\bar{\rho}\tilde{u}_j\tilde{u}_i\right) = -\frac{\partial \bar{p}}{\partial x_i} + \frac{\partial}{\partial x_j}\left(2(\mu+\mu_t)\tilde{S}_{ji}\right),$$

$$\frac{\partial}{\partial t}\left[\bar{\rho}\left(\tilde{e}+\frac{1}{2}\tilde{u}_i\tilde{u}_i\right)\right] + \frac{\partial}{\partial x_j}\left[\bar{\rho}\tilde{u}_j\left(\tilde{h}+\frac{1}{2}\tilde{u}_i\tilde{u}_i\right)\right] = \frac{\partial}{\partial x_j}\left(2(\mu+\mu_t)\tilde{S}_{ji}\tilde{u}_i\right) + \frac{\partial}{\partial x_j}\left[\left(\frac{\mu}{\mathrm{Pr}}+\frac{\mu_t}{\mathrm{Pr}_t}\right)\frac{\partial \tilde{h}}{\partial x_j}\right],$$

$$\frac{\partial}{\partial t}(\bar{\rho}\nu_{\mathrm{sa}}) + \frac{\partial}{\partial x_j}(\bar{\rho}\tilde{u}_j\nu_{\mathrm{sa}}) = c_{b1}S_{\mathrm{sa}}\bar{\rho}\nu_{\mathrm{sa}} - c_{w1}f_w\bar{\rho}\left(\frac{\nu_{\mathrm{sa}}}{d}\right)^2 + \frac{1}{\sigma}\frac{\partial}{\partial x_k}\left[(\mu+\bar{\rho}\nu_{\mathrm{sa}})\frac{\partial \nu_{\mathrm{sa}}}{\partial x_k}\right] + \frac{c_{b2}}{\sigma}\bar{\rho}\frac{\partial \nu_{\mathrm{sa}}}{\partial x_k}\frac{\partial \nu_{\mathrm{sa}}}{\partial x_k},$$

where $\tilde{[\,]}$ denotes the Favre-average and $\bar{[\,]}$ denotes the Reynolds average. Furthermore, ρ is the density; u_i is the i^{th} velocity component; e is the internal energy; p is the pressure; h is the enthalpy; S_{ji} is the deviatoric part of the strain-rate tensor; μ is the fluid viscosity; μ_t is the eddy viscosity; d is the distance to the nearest no-slip wall; and ν_{sa} is the SA state variable. A number of additional relationships are required to close the equations. First, the fluid is assumed to be a calorically perfect gas with a *constant* viscosity. Thus,

$$\bar{p} = \bar{\rho}R\tilde{T}, \quad \tilde{e} = c_v\tilde{T}, \quad \tilde{h} = c_p\tilde{T},$$

where $R = c_p - c_v$, and c_p and c_v are constant. Second, the turbulence model has the following algebraic closure relationships:

$$\mu_t = \bar{\rho}\nu_{\mathrm{sa}}f_{v1}, \qquad f_{v1} = \frac{\chi^3}{\chi^3+c_{v1}^3}, \qquad f_{v2} = 1-\frac{\chi}{1+\chi f_{v1}}, \quad \chi = \frac{\nu_{\mathrm{sa}}}{\nu},$$

$$f_w = g\left(\frac{1+c_{w3}^6}{g^6+c_{w3}^6}\right)^{1/6}, \quad g = r + c_{w2}\left(r^6-r\right), \qquad r = \frac{\nu_{\mathrm{sa}}}{S_{\mathrm{sa}}\kappa^2 d^2}.$$

The remaining closure function, S_{sa}, is slightly different from that specified in the original model. In the original formulation, S_{sa} is given by

$$S_{\mathrm{sa}} = \Omega + \frac{\nu_{\mathrm{sa}}}{\kappa^2 d^2}f_{v2}, \tag{1}$$

where Ω is the magnitude of the vorticity. Following Allmaras,[17,18] this definition is modified to avoid the possibility of S_{sa} being negative due to f_{v2} being negative. In particular, letting

$$S_{m0} = \frac{\nu_{\mathrm{sa}}}{\kappa^2 d^2}f_{v2},$$

S_{sa} is given by

$$S_{\mathrm{sa}} = \Omega + S_m,$$

where

$$S_m = \begin{cases} S_{m0}, & S_{m0} \geq -c_{v2}\Omega \\ \dfrac{\Omega(c_{v2}^2\Omega + c_{v3}S_{m0})}{((c_{v3}-2c_{v2})\Omega - S_{m0})}, & \text{otherwise.} \end{cases}$$

III. Review of Existing Physically-Based Manufactured Solutions

In this section, the physically-motivated solutions of Eça et al.[12–14] are reviewed and analyzed. Eça and co-workers[12–14] proposed three manufactured solutions for the incompressible version of the SA model. These solutions are of interest here because they are nominally intended to mimic the behavior of a stationary, two-dimensional boundary layer. However, using the PARNASSOS flow solver,[19] the expected second-order accuracy was observed for only one solution,[14] leading the authors to conclude that "the construction of MSs [manufactured solutions] for turbulence models is a delicate matter." The analysis shown here is intended to illuminate the features of the Eça solutions that cause difficulties so that these difficulties can be avoided in the current effort.

The three solutions developed by Eça and co-workers share the same manufactured velocity and pressure fields, but only the velocity field is required for the analysis shown here. Specifically, the manufactured velocity field is given by

$$u = \mathrm{erf}(\eta),$$
$$v = \frac{1}{\sigma\sqrt{\pi}}(1 - e^{-\eta^2}),$$

where u is the streamwise velocity component, v is the wall-normal velocity component, $\eta = \frac{\sigma y}{x}$, and σ is a constant. As noted by Eça et al.,[14] this velocity profile is not realistic for a wall-bounded turbulent flow. In particular, it exhibits no logarithmic layer.

The distinguishing feature of the three manufactured solutions is the SA state variable, ν_{sa}. The solutions are labeled "MS4", "MS2", and "MS1" corresponding to the near-wall behavior of ν_{sa}. Specifically, the manufactured SA state is given by

$$\begin{aligned}
\text{MS4}: &\quad \nu_{\mathrm{sa}} = \frac{1}{4}\tilde{\nu}_{\max}\eta_\nu^4 e^{2-\eta_\nu^2},\\
\text{MS2}: &\quad \nu_{\mathrm{sa}} = \tilde{\nu}_{\max}\eta_\nu^2 e^{1-\eta_\nu^2},\\
\text{MS1}: &\quad \nu_{\mathrm{sa}} = \tilde{\nu}_{\max}\sqrt{2}\eta_\nu e^{0.5-\eta_\nu^2},
\end{aligned}$$

where $\eta_\nu = \frac{\sigma_\nu y}{x}$, $\sigma_\nu = 2.5\sigma$, and $\tilde{\nu}_{\max} = 10^3\nu$. Thus, for $y \ll 1$,

$$\begin{aligned}
\text{MS4}: &\quad \nu_{\mathrm{sa}} \propto y^4,\\
\text{MS2}: &\quad \nu_{\mathrm{sa}} \propto y^2,\\
\text{MS1}: &\quad \nu_{\mathrm{sa}} \propto y.
\end{aligned}$$

These solutions are analyzed individually in the following sections.

III.A. MS4

Eça et al.[14] show suboptimal convergence (approximately $\mathcal{O}(h)$) using MS4. This behavior is attributed to the y^4 behavior of ν_{sa} in the near-wall region.[14] In an attempt to understand this problem in more detail, the stability of the SA equation linearized about MS4 is examined. It is shown that, near the wall, the SA equation is linearly unstable about MS4. It is postulated that this instability is responsible for the bump observed in the numerical solutions reported by Eça et al. (see Figure 4 in reference[14]).

Let m denote the manufactured solution, and let ϵ denote a small perturbation of this solution. Then, letting

$$\nu_{\mathrm{sa}} = m + \epsilon,$$

the incompressible SA equation requires that

$$\begin{aligned}
\frac{\partial}{\partial t}(m+\epsilon) + \bar{u}_j\frac{\partial}{\partial x_j}(m+\epsilon) = c_{b1}\tilde{S}(m+\epsilon) - c_{w1}f_w\left(\frac{m+\epsilon}{d}\right)^2\\
+ \frac{1}{\sigma}\frac{\partial}{\partial x_k}\left[(\nu+m+\epsilon)\frac{\partial}{\partial x_k}(m+\epsilon)\right] + \frac{c_{b2}}{\sigma}\frac{\partial(m+\epsilon)}{\partial x_k}\frac{\partial(m+\epsilon)}{\partial x_k},
\end{aligned}$$

where $\tilde{S}$ denotes the original form of S_{sa}, as given in (1), since Eça and co-workers use the original form of the model.

Neglecting terms that are higher-order in ϵ, it is straightforward to show that the linearized SA equation is

$$\begin{aligned}
\frac{\partial\epsilon}{\partial t} + \bar{u}_j\frac{\partial\epsilon}{\partial x_j} = c_{b1}\tilde{S}\epsilon + c_{b1}\frac{\partial\tilde{S}}{\partial\nu_{\mathrm{sa}}}\epsilon m - 2c_{w1}f_w\frac{m\epsilon}{d^2} - c_{w1}\frac{\partial f_w}{\partial\nu_{\mathrm{sa}}}\epsilon\left(\frac{m}{d}\right)^2\\
+ \frac{1}{\sigma}\left[\frac{\partial}{\partial x_k}\left((\nu+m)\frac{\partial\epsilon}{\partial x_k}\right) + \frac{\partial}{\partial x_k}\left(\epsilon\frac{\partial m}{\partial x_k}\right)\right] - 2\frac{c_{b2}}{\sigma}\frac{\partial m}{\partial x_k}\frac{\partial\epsilon}{\partial x_k}.
\end{aligned}$$

Making a boundary layer approximation, it is assumed that $\frac{\partial}{\partial x} \ll \frac{\partial}{\partial y}$. Note that this assumption is satisfied by the manufactured solutions under consideration. Furthermore, considering only the very near-wall region, the convection term can be neglected. These approximations lead to the following equation, which is valid for small perturbations of all of the Eça manufactured solutions very close to the wall (i.e., as $y \to 0$):

$$\begin{aligned}\frac{\partial \epsilon}{\partial t} &= c_{b1}\tilde{S}\epsilon + c_{b1}\frac{\partial \tilde{S}}{\partial \nu_{\text{sa}}}\epsilon m - 2c_{w1}f_w\frac{m\epsilon}{d^2} - c_{w1}\frac{\partial f_w}{\partial \nu_{\text{sa}}}\epsilon\left(\frac{m}{d}\right)^2 \\ &\quad + \frac{1}{\sigma}\left[\frac{\partial}{\partial y}\left((\nu+m)\frac{\partial \epsilon}{\partial y}\right) + \frac{\partial}{\partial y}\left(\epsilon\frac{\partial m}{\partial y}\right)\right] - 2\frac{c_{b2}}{\sigma}\frac{\partial m}{\partial y}\frac{\partial \epsilon}{\partial y}. \end{aligned} \tag{2}$$

To continue the analysis, the terms of (2) are examined as $y \to 0$ with m set to ν_{sa} from MS4. For brevity, the details are omitted. The result is that, after neglecting terms that are higher-order in y, (2) becomes

$$\frac{\partial \epsilon}{\partial t} = c_{b1}\Omega_w\epsilon + \frac{1}{\sigma}\nu\frac{\partial^2 \epsilon}{\partial y^2} = \mathcal{L}\epsilon,$$

where $\mathcal{L} \equiv c_{b1}\Omega_w + \frac{\nu}{\sigma}\frac{\partial^2}{\partial y^2}$ and Ω_w is the magnitude of the vorticity at the wall. Since $\sigma c_{b1}\Omega_w/\nu > 1$, the operator $\mathcal{L}$ has positive eigenvalues. Components of the perturbation ϵ that are aligned with eigenfunctions corresponding to these eigenvalues are unstable and will tend to grow. Thus, while the manufactured solution is still an exact solution of the governing equations, depending on the details of perturbations introduced by the discretization and whether any nearby stable solutions exist, the numerical solution on a given mesh may converge to something quite different, as observed by Eça et al.[14]

Thus, it appears that this instability may be the cause of the difficulties reported using MS4. Furthermore, the root cause of the instability is the fact that the near-wall balance in the SA equation for MS4 does not resemble that expected for actual solutions of the SA model. In particular, both production and dissipation tend to zero as $y \to 0$. The model is designed such that these terms should tend to constants.[7] More importantly, for MS4, the ratio of dissipation to production also goes to zero as $y \to 0$. The result is that there is far too little dissipation near the wall, and dissipation vanishes entirely in the near-wall, linearized SA equation, leading to the instability. This qualitative mismatch with the expected behavior of actual SA solutions and the resulting instability make MS4 a poor candidate for verification using the MMS.

III.B. MS2

MS2 has $\nu_{\text{sa}} \propto y^2$ as $y \to 0$. This behavior is not as extreme as MS4, and MS2 does not have some of the pathological features of MS4. Namely, the ratio of dissipation to production does not go to zero at the wall, and the dissipation term does not disappear from the linearized, near-wall SA equation. Using MS2, Eça et al.[14] report that the expected second-order accuracy is observed. Thus, it appears that this solution does not cause any numerical difficulties. However, the solution still has features that are qualitatively different from the expected near-wall behavior of actual SA solutions.

Specifically, the behavior of the production and dissipation terms as $y \to 0$ is different from that expected for real solutions. As noted in Section III.A, real solutions of the SA equations are expected to give production and dissipation terms that go to constants at the wall. For MS2, these terms tend to zero.

Furthermore, the components of the production are not exercised in a manner that resembles the expected behavior of real SA solutions. As shown in (3), the production term is composed of two parts:

$$P = P_\Omega + P_{mod} = \underbrace{c_{b1}\Omega\nu_{\text{sa}}}_{\text{Vorticity}} + \underbrace{c_{b1}\frac{\nu_{\text{sa}}^2 f_{v2}}{\kappa^2 d^2}}_{\text{Modification}}. \tag{3}$$

The model is designed such that the vorticity term dominates in the logarithmic layer, while the modification changes the near-wall behavior such that ν_{sa} maintains the log layer profile all the way to the wall. For actual solutions of the SA model, $\nu_{\text{sa}} \propto y$ near the wall, which implies that P_{mod} is dominant:

$$\frac{P_\Omega}{P_{mod}} \to 0 \quad \text{as} \quad y \to 0,$$

since P_Ω goes to zero while P_{mod} goes to a constant. Alternatively, for MS2, since $\nu_{\text{sa}} \propto y^2$, this limiting behavior is not observed. Instead, for $x > 0$,

$$\frac{P_\Omega}{P_{mod}} \to \frac{\Omega_w\kappa^2 x}{\tilde{\nu}_{max}\sigma_\nu^2} \quad \text{as} \quad y \to 0.$$

For the domain and parameter values used by Eça et al.,[14] the vorticity part of the production is always dominant.

Thus, as with MS4, MS2 does not exercise the model in a manner similar to real SA solutions. As noted in Section I, this situation is suboptimal because it may lead to false success in a verification test. Specifically, because P_{mod} is dominated by P_Ω, an implementation error in P_{mod} may not become apparent until very fine meshes. If optimal accuracy were observed before this error became important, one might stop the mesh refinement and falsely conclude that the test was a success. While this "false positive" may be a low probability event (and it has not been explored computationally here), it is better to develop a manufactured solution that has the correct near-wall behavior.

III.C. MS1

While the asymptotic behaviors of MS2 and MS4 as $y \to 0$ do not agree with real solutions of the SA model, MS1 does have the correct $\nu_{\text{sa}} \propto y$ behavior for small y. However, Eça et al.[14] report that, while the pointwise error in ν_{sa} at a number of monitored points shows second-order convergence, the RMS error does not. In fact, the RMS error does not achieve a consistent convergence rate. The monitored points, where optimal pointwise results are obtained, have $y \geq 1.43 \times 10^{-3} \Rightarrow y^+ \gtrsim 3$. Thus, it appears that the problems in the RMS stem from the behavior very near the wall. Eça and co-authors attribute the problem to the dissipation term in the SA equation,[14] but it is not clear what about this term is problematic. Here, the dissipation and production terms in the near-wall region are examined. Two causes for concern are uncovered: sign changes in the dissipation and production terms and unresolved features in the dissipation.

Figure 1 shows the SA dissipation term as a function of y^+ at $x = 0.75$. For $y^+ \geq 2$, the behavior is smooth and should be resolved on any reasonable mesh. Alternatively, near the wall, there are very small features, particularly in the dissipation. For example, the dissipation changes by approximately a

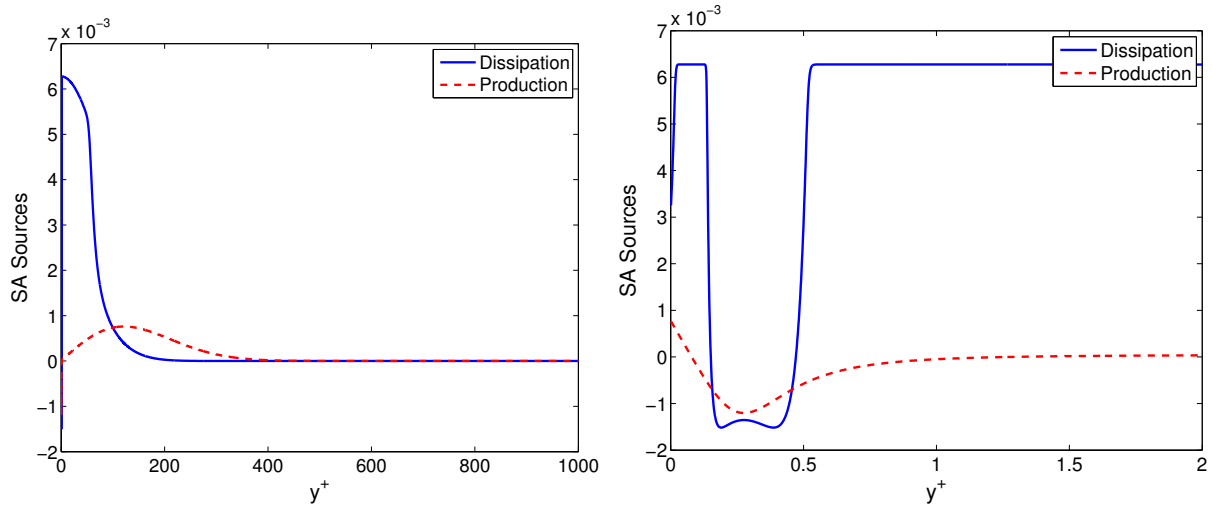

(a) $y^+ < 1000$. (b) $y^+ < 2$.

Figure 1. SA dissipation ($c_{w1} f_w (\nu_{\text{sa}}/d)^2$) and production ($c_{b1} \tilde{S} \nu_{\text{sa}}$) for MS1 as a function of y^+ at $x = 0.75$.

factor of two from the wall ($y^+ = 0$) to $y^+ \approx 0.03$. This feature is not resolved on even the finest meshes (401×401 nodes) used by Eça and co-workers, where the first node above the wall is at $y \approx 6.3 \times 10^{-5}$, which corresponds to $y^+ \approx 0.15$ at $x = 0.75$.

Also note that both the production and dissipation change signs near the wall. Strictly speaking, these sign changes are a problem with the model, not the manufactured solution. They happen because f_{v2} is negative in a region where the vorticity is too small to make the net $\tilde{S}$ positive. It is possible that these features are related to the results obtained using MS1.

While these sign changes are eliminated using the modified S_{sa} formulation shown in Section II, the small features near the wall are still a cause for concern. Whether or not they are ultimately responsible for the convergence anomalies observed using MS1, these kind of features are not expected for real solutions of the

SA model. Their presence here indicates that, at the wall, ν_{sa} is growing too rapidly with y.

In the SA model, the blending functions that are responsible for the transition from viscous sublayer to logarithmic layer behavior are based on the variable $\chi = \nu_{\text{sa}}/\nu$. The SA model is designed to produce $\chi \approx \kappa y^+$ in the viscous sublayer and log layer. Alternatively, MS1 has

$$\begin{aligned}\chi &= \frac{\tilde{\nu}_{max}}{\nu}\sqrt{2}\eta_\nu \exp\left(\frac{1}{2} - \eta_\nu^2\right) \\ &\approx \frac{\tilde{\nu}_{max}}{u_\tau}\frac{\sqrt{2}\sigma_\nu e^{1/2}}{x}y^+ \quad \text{for} \quad y \ll 1.\end{aligned}$$

Thus, for the values of the constants used by Eça et al.,[14] χ grows approximately 37.85 times faster than the expected SA solution at $x = 0.5$ and 26.77 times faster at $x = 1.0$. This rapid growth implies that the majority of the variation of the blending functions happens for $y^+ < 1$. Figure 2 compares the functions f_{v1}, f_{v2}, and f_w for MS1 and the expected SA solution (using the manufactured velocity to compute Ω). Observe

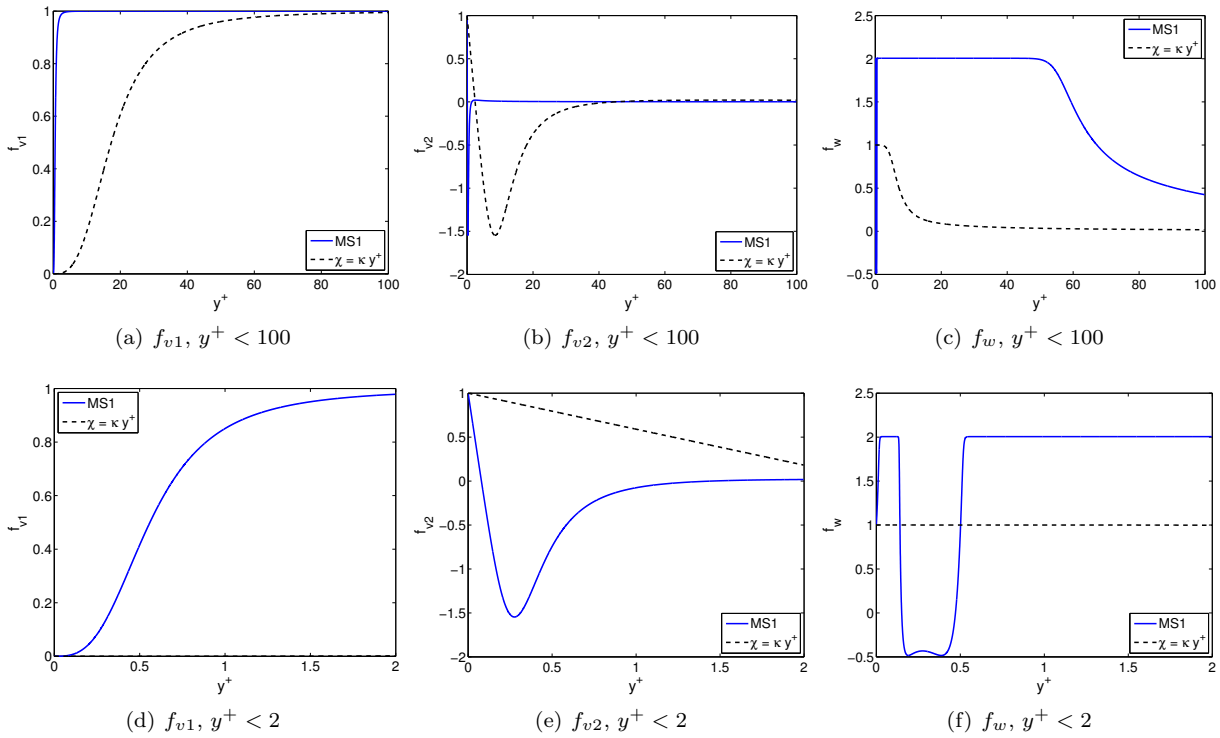

(a) f_{v1}, $y^+ < 100$ (b) f_{v2}, $y^+ < 100$ (c) f_w, $y^+ < 100$

(d) f_{v1}, $y^+ < 2$ (e) f_{v2}, $y^+ < 2$ (f) f_w, $y^+ < 2$

Figure 2. Near-wall behavior of SA closure functions for MS1 and expected SA solution behavior ($\chi = \kappa y^+$) at $x = 0.75$.

that MS1 has substantial variability for $y^+ < 1$ in all three functions. The dissipation term closure function f_w is particularly nasty, going from one at the wall to approximately 2.005 at $y^+ = 0.03$. The behavior of f_w is directly responsible for the behavior of the dissipation shown in Figure 1.

While it is not entirely clear that these near-wall features are responsible for the behavior observed by Eça et al.,[14] it is reasonable to expect that asymptotic order of accuracy for the numerical scheme will not be observed when parts of the governing equations are not well-resolved. Furthermore, the fact that the source terms have length scales significantly smaller than those expected in real simulations is clearly undesirable for a physically realistic manufactured solution.

IV. Manufactured Solutions

This section details the new manufactured solutions developed in this work. Specifically, Section IV.A describes the sinusoidal form, and Section IV.B describes the boundary layer-based form. Both solutions developed here, as well as a number of other manufactured solutions that are of interest to the aerospace community, are implemented in the `MASA` library.[16] The library is discussed further in Section V.

IV.A. Sinusoidal-based Manufactured Solution

Following Roy, Smith and Ober,[15] the general form of the manufactured solution for the primitive variables is taken to be a function of sines and cosines in x and y:

$$\phi(x,y) = \phi_0 + \phi_x\, f_s\left(\frac{a_{\phi x}\pi x}{L}\right) + \phi_y\, f_s\left(\frac{a_{\phi y}\pi y}{L}\right),$$

where $\phi = \bar{\rho}$, $\tilde{u}$, $\tilde{v}$, $\bar{p}$ or ν_{sa}, and $f_s(\cdot)$ denotes the sine or cosine function. Here, ϕ_x and ϕ_y are constants and the subscripts do not denote differentiation.

Applying this form to the FANS–SA primitive state variables, the manufactured solution is as follows:

$$\begin{aligned}
\bar{\rho} &= \rho_0 + \rho_x \sin\left(\frac{a_{\rho x}\pi x}{L}\right) + \rho_y \cos\left(\frac{a_{\rho y}\pi y}{L}\right),\\
\tilde{u} &= u_0 + u_x \sin\left(\frac{a_{ux}\pi x}{L}\right) + u_y \cos\left(\frac{a_{uy}\pi y}{L}\right),\\
\tilde{v} &= v_0 + v_x \cos\left(\frac{a_{vx}\pi x}{L}\right) + v_y \sin\left(\frac{a_{vy}\pi y}{L}\right),\\
\bar{p} &= p_0 + p_x \cos\left(\frac{a_{px}\pi x}{L}\right) + p_y \sin\left(\frac{a_{py}\pi y}{L}\right),\\
\nu_{\text{sa}} &= \nu_{\text{sa}0} + \nu_{\text{sa}x} \cos\left(\frac{a_{\nu_{\text{sa}}x}\pi x}{L}\right) + \nu_{\text{sa}y} \cos\left(\frac{a_{\nu_{\text{sa}}y}\pi y}{L}\right),
\end{aligned}$$

where $(\cdot)_0$, $(\cdot)_x$, $(\cdot)_y$, $a_{\cdot x}$, $a_{\cdot y}$, and L are user-specified parameters. The default `MASA` values for these parameters are given in Appendix A.A.

IV.B. Physically-based Manufactured Solution

The second manufactured solution developed here is intended to satisfy three goals. First, it should have a reasonable velocity profile structure for a turbulent boundary layer. Namely, it should have both a viscous sublayer and a logarithmic layer. Second, to avoid issues like those discussed for MS4 and MS2, it should have the correct asymptotic structure for ν_{sa} as $y \to 0$. Third, to avoid potential problems like those discussed for MS1, it should not have very small-scale features in the SA closure functions or source terms near the wall. To accomplish these goals, the solution was developed using well-known correlations for compressible turbulent boundary layers and the expected behavior of the SA state variable.

Throughout this section, typical boundary layer notation is used. Thus, $(\cdot)_\infty$ denotes a quantity evaluated at the boundary layer edge, and $(\cdot)_w$ denotes a quantity evaluated at the wall. A list of parameters of the manufactured solution is detailed in Appendix A.B.

IV.B.1. The Velocity Field

To set the streamwise velocity, models for the equivalent incompressible boundary layer profile are constructed and transformed using the van Driest transformation.[20,21] Using the adiabatic form of the van Driest transformation, the mean streamwise velocity is given by

$$\tilde{u} = \frac{u_\infty}{A}\sin\left(\frac{A}{u_\infty}u_{eq}\right),$$

where u_∞, $A = \sqrt{1 - T_\infty/T_w}$, T_∞, and T_w are constants, and u_{eq} is the van Driest equivalent velocity. The van Driest velocity can be written as

$$u_{eq} = u_\tau u^+_{eq},$$

where $u_\tau = \sqrt{\tau_w/\rho_w}$ is the friction velocity and u^+_{eq} is the non-dimensional van Driest velocity. Thus, to specify the velocity, one must specify u_τ and u^+_{eq}. The friction velocity can be determined from the skin friction coefficient as follows:

$$u_\tau \equiv \sqrt{\frac{\tau_w}{\rho_w}} = u_\infty\sqrt{\frac{c_f}{2}}.$$

The skin friction coefficient is set using the compressibility transformation idea of Spalding and Chi[22] and a correlation for the incompressible skin friction. Specifically,

$$c_f = \frac{1}{F_c}c_{f,inc}\left(\frac{1}{F_c}Re_x\right),$$

where $F_c = (T_w/T_\infty - 1)/\left(\sin^{-1} A\right)^2$ is a constant and $c_{f,inc}$ is a correlation for the incompressible skin friction. The 1/7th power law is used for the incompressible skin friction coefficient. Thus,

$$c_{f,inc}(Re_x) = C_{cf} Re_x^{-1/7},$$

where C_{cf} is a constant and $Re_x = \rho_\infty u_\infty x/\mu$.

Finally, to complete the manufactured solution, u^+_{eq} is set using the velocity profile model of Cebeci and Bradshaw:[23]

$$u^+_{eq} = \frac{1}{\kappa}\log\left(1+\kappa y^+\right) + C_1\left[1 - e^{-y^+/\eta_1} - \frac{y^+}{\eta_1}e^{-y^+ b}\right],$$

where κ, $C_1 = -(1/\kappa)\log(\kappa) + C$, C, η_1 and b are constants and

$$y^+ \equiv \frac{y}{\ell_v}, \quad \text{and} \quad \ell_v \equiv \frac{\nu_w}{u_\tau}.$$

This completes the specification of the streamwise velocity.

Based on a crude order of magnitude analysis of the continuity equation, the mean wall-normal velocity is set to

$$\tilde{v} = -\eta_v \frac{du_\tau}{dx} y,$$

where η_v is a user-specified parameter.

IV.B.2. The Thermodynamic State

The mean temperature is set using the following temperature-velocity relation:[21]

$$\tilde{T} = T_\infty\left[1 + r_T\frac{\gamma-1}{2}M_\infty^2\left(1 - \left(\frac{\tilde{u}}{u_\infty}\right)^2\right)\right],$$

where M_∞ is the edge Mach number, r_T is the recovery factor, and γ is the ratio of specific heats. Note that the constant T_w is defined as $T_w = T(\tilde{u} = 0)$. The pressure is assumed to be constant in both the streamwise and wall-normal directions. Thus, it is simply a constant, denoted p_0. Finally, the density is computed from the ideal gas equation:

$$\bar{\rho} = \frac{p_0}{R\tilde{T}}.$$

IV.B.3. The SA State

The SA model is designed such that $\nu_{\text{sa}} = \kappa u_\tau y$ in the inner region of an incompressible boundary layer.[7] Even though the solution here is compressible, this form is used near the wall. A quadratic term is added to make the solution formally nonlinear in y. Specifically, the SA state variable is given by

$$\nu_{\text{sa}} = \kappa u_\tau y - \alpha y^2,$$

where α is a constant.

IV.B.4. Solution and Source Term Plots

This section shows plots of the manufactured solution and source terms. The plots indicate that the manufactured solution achieves the desired goals of having a realistic turbulent velocity profile and of having the correct behavior in the SA model near the wall. The figures shown here correspond to the "high Re" case used in Section VI.B.2 to verify FIN-S.

Figure 3 shows the manufactured velocity profile. By construction, the Van Driest transformed velocity profile has the expected structure of the near-wall region of a turbulent boundary layer, showing both the viscous sublayer and log layer behavior.

Figure 4 shows the manufactured temperature and density profiles. While the variations in $\bar{\rho}$ and $\tilde{T}$ are not dramatic, these variations are intended to be large enough to uncover programming errors that would not be uncovered using constants for $\bar{\rho}$ and $\tilde{T}$.

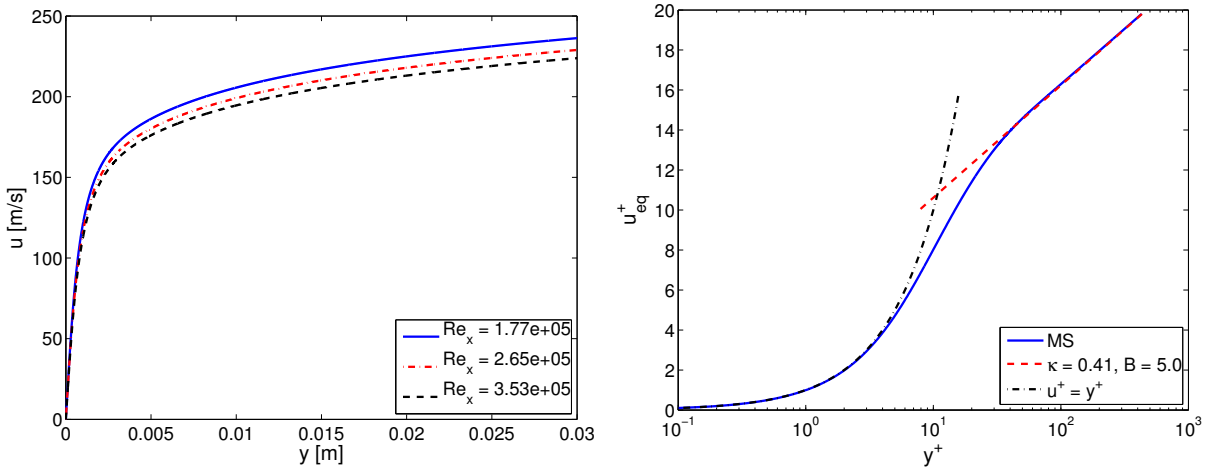

Figure 3. Manufactured velocity profiles. Left: Variation of dimensional velocity with Re_x. Right: Non-dimensional (wall units) Van Driest transformed velocity.

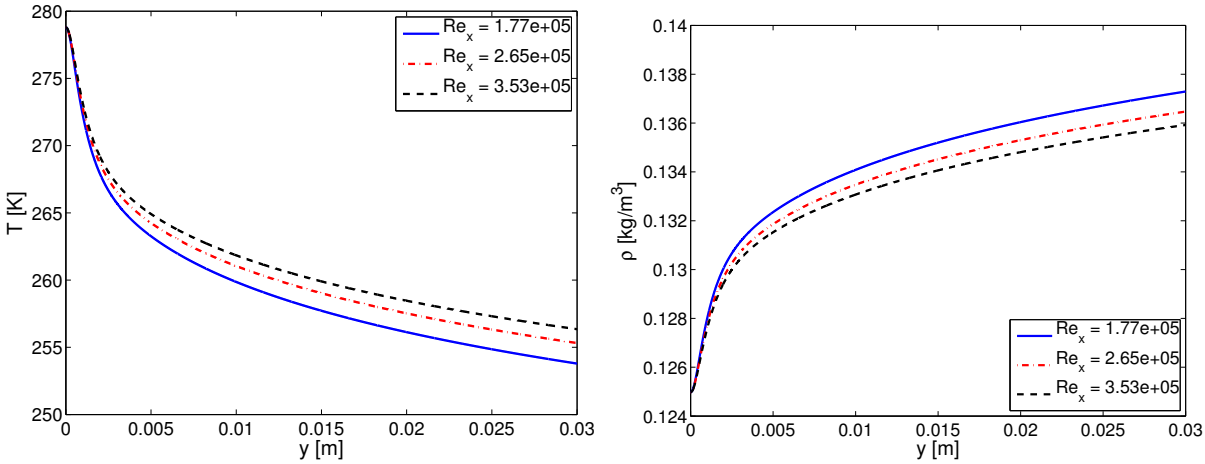

Figure 4. Manufactured temperature (left) and density (right) profiles.

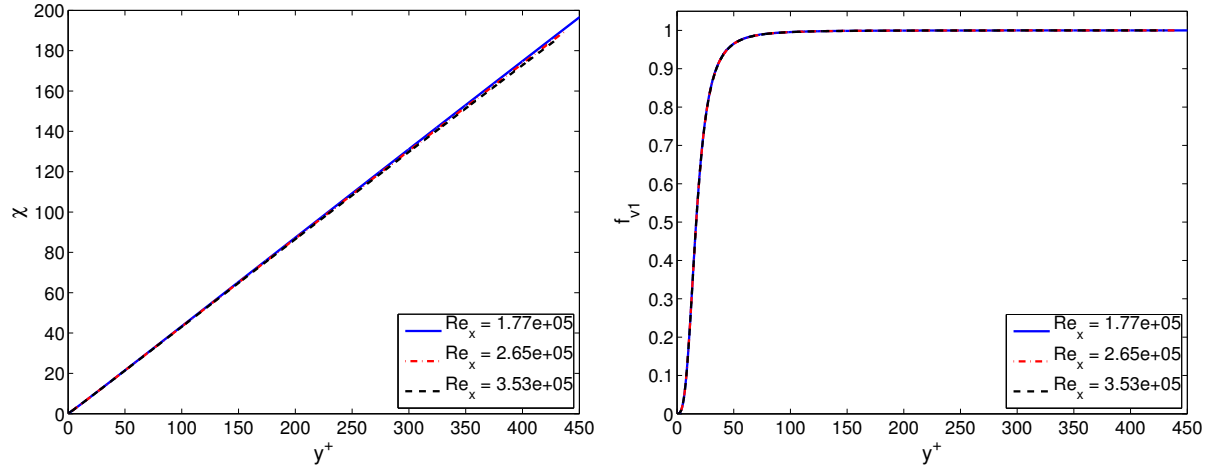

Figure 5. Manufactured χ (left) and f_{v1} (right) profiles.

Figure 5 shows the profiles of χ and f_{v1} computed from the manufactured ν_{sa}. The χ variable is nearly equal to κy^+ over the entire domain. Furthermore, while the f_{v1} variable does show strong variation near the wall, this variation is consistent with that expected in real simulations. For instance, $f_{v1} \approx 0.9$ at $y^+ \approx 35$, as opposed to MS1, where $f_{v1} \approx 0.9$ at $y^+ \approx 1.25$ (see Figure 2).

Figure 6 shows the SA equation budget at $x = 0.75$m. There are two important features of the SA

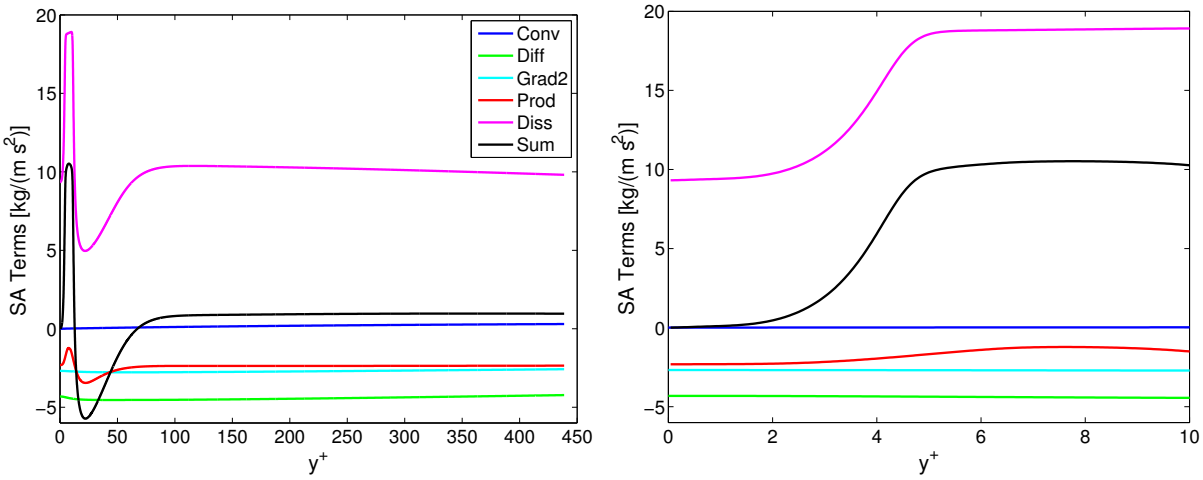

(a) Full domain (b) Near wall

Figure 6. SA equation budget for the wall-bounded flow manufactured solution on a line normal to the wall at $x = 0.75$. The budget is split into five terms: "Conv" ($\nabla \cdot (\bar{\rho}\vec{u}\nu_{\text{sa}})$), "Diff" ($-\frac{1}{\sigma}\nabla \cdot ((\mu + \rho\nu_{\text{sa}})\nabla\nu_{\text{sa}})$), "Grad2" ($-\frac{c_{b2}}{\sigma}\rho\nabla\nu_{\text{sa}} \cdot \nabla\nu_{\text{sa}}$), "Prod" ($-c_{b1}S_{\text{sa}}\rho\nu_{\text{sa}}$), and "Diss" ($c_{w1}f_w\rho\left(\frac{\nu_{\text{sa}}}{d}\right)^2$). "Sum" is the sum of these terms and represents the source term added to the right-hand side in the MMS.

budget. First, the production ("Prod") and dissipation ("Diss") terms have the correct near-wall behavior—i.e., both terms go to constants at the wall and the wall values are maintained well into the viscous sublayer. Second, the total residual that becomes the source term in the MMS—denoted "Sum" in the figures—is small over much of the layer. Specifically, well inside the viscous sublayer ($y^+ < 2$) and also in the logarithmic layer ($y^+ > 50$), the source term is small relative to other terms in the SA equation, indicating that the manufactured solution nearly satisfies the SA equation in these regions. The source term is largest in the buffer region between these two layers. In this region, the correlations used to build the manufactured solution do not correctly represent the actual flow or the FANS-SA model solution. Thus, it is not surprising that the source term is larger in this region.

V. The `MASA` Library

The Manufactured Analytical Solution Abstraction (`MASA`) library is designed to act as a central repository and standardized API for manufactured solutions. It is intended to cover a wide variety of physics (fluids, thermodynamics, etc.) and support almost any solution form (trigonometric, polynomial, etc.).

Manufactured solutions currently incorporated in `MASA` include the heat, Navier-Stokes, and Euler equations, as well as the subject of this paper: Favre-averaged Navier-Stokes with the Spalart-Allmaras turbulence model for free shear flow. The wall-bounded MMS discussed in this paper is included in the latest `MASA` release, 0.40.

Interfacing a codebase with the `MASA` API is relatively straightforward. For example, the manufactured analytical solution for the density can be evaluated at a point (x, y) by calling `masa_eval_exact_rho(Scalar x, Scalar y)`, where Scalar can be a float, double, or long double. Likewise, the value of the source term for the conservation of mass equation at (x, y) would be returned by `masa_eval_source_rho(Scalar x, Scalar y)`.

`MASA` provides default values for the parameters required for initializing the manufactured solutions. As discussed at the beginning of Section IV, care was taken to ensure that default parameters are selected in such a way as to produce solutions that are physically realizable, and fully exercise all the terms in the

equations.

MASA is written in C++, and provides C/C++, and Fortran90 interfaces. The library is open-source and publicly released under the Lesser GNU Public License version 0.21. The current version, MASA 0.33, is available at https://red.ices.utexas.edu/projects/software. More details on the library will be available in the MASA publication.[16]

VI. FIN-S Mesh Refinement Study Results

The manufactured solutions described in Section IV have been used as part of verification of the FIN-S flow solver. FIN-S is a compressible Navier-Stokes flow solver[8,9] built upon the libMesh finite element library.[24] Spatial discretization is accomplished using the streamline-upwind Petrov Galerkin (SUPG) finite element method. In this work, standard piecewise bilinear Lagrange basis functions defined on quadrilateral elements are used. Thus, the scheme is expected to produce solutions with errors that converge to zero like $\mathcal{O}(h^2)$ in the L_2 norm.

VI.A. Sinusoidal-based Manufactured Solution

Results using the sinusoidal-based manufactured solution have been obtained for two different settings of the parameters. These two different settings lead to low Re and high Re cases that exercise the code in different ways. In both cases, the simulation domain is the unit square.

VI.A.1. Low Re

For the low Re case, the parameters are set as follows:

$$\mu = 2.0\tfrac{\text{kg}}{\text{ms}}, \quad u_0 = 1.0\tfrac{\text{m}}{\text{s}}, \quad u_y = 0.8\tfrac{\text{m}}{\text{s}}, \quad p_0 = 100\tfrac{\text{N}}{\text{m}^2}.$$

All other parameters are set to their default values, as given in Appendix A.A. These parameters settings lead to a very low Re case. Specifically, the element Reynolds number based on the magnitude of the velocity plus the speed of sound and the element characteristic length is everywhere less than one. Thus, this case exercises the SUPG discretization in the diffusion-dominated regime.

A mesh refinement study over a sequence of 6 uniform, isotropic meshes has been performed. The coarse mesh is 16×16 elements. Each subsequent mesh is refined by a factor of 2 in both directions, leading to a fine mesh of 512×512 elements. Figure 7 shows the resulting error, measured in the L_2 norm, as a function of mesh refinement. The figure shows that the asymptotic convergence rate is $\mathcal{O}(h^2)$. On the initial coarse meshes, the convergence rate is somewhat suboptimal, which is consistent with what is expected for the SUPG scheme implemented in FIN-S in the transition between the convection and diffusion dominated limits.

VI.A.2. High Re

For the high Re case, the parameters are set as follows:

$$\begin{aligned} &\mu = 1 \times 10^{-3}\tfrac{\text{kg}}{\text{ms}}, \quad u_0 = 3 \times 10^{3}\tfrac{\text{m}}{\text{s}}, \qquad u_y = 50\tfrac{\text{m}}{\text{s}}, \qquad v_y = 100\tfrac{\text{m}}{\text{s}}, \\ &p_0 = 1 \times 10^{5}\tfrac{\text{N}}{\text{m}^2}, \quad p_x = 1 \times 10^{3}\tfrac{\text{N}}{\text{m}^2}, \quad p_y = 1 \times 10^{3}\tfrac{\text{N}}{\text{m}^2}. \end{aligned}$$

All other parameters are set to their default values. These parameters settings lead to a high Re case, where the element Reynolds numbers are greater than one. Thus, this case exercises the SUPG scheme in the convection-dominated regime.

A mesh refinement study was conducted using the same meshes as for the low Re case. Figure 8 shows the resulting error, measured in the L_2 norm, as a function of mesh refinement. Clearly, $\mathcal{O}(h^2)$ convergence is observed.

VI.B. Physically-based Manufactured Solution

As with the sinusoidal-based case, results using the physically-based manufactured solution have been obtained for two different settings of the parameters, leading to low and high Re cases. In both cases, the simulation domain is the rectangle $[0.5, 1]\text{m} \times [0, 0.03]\text{m}$.

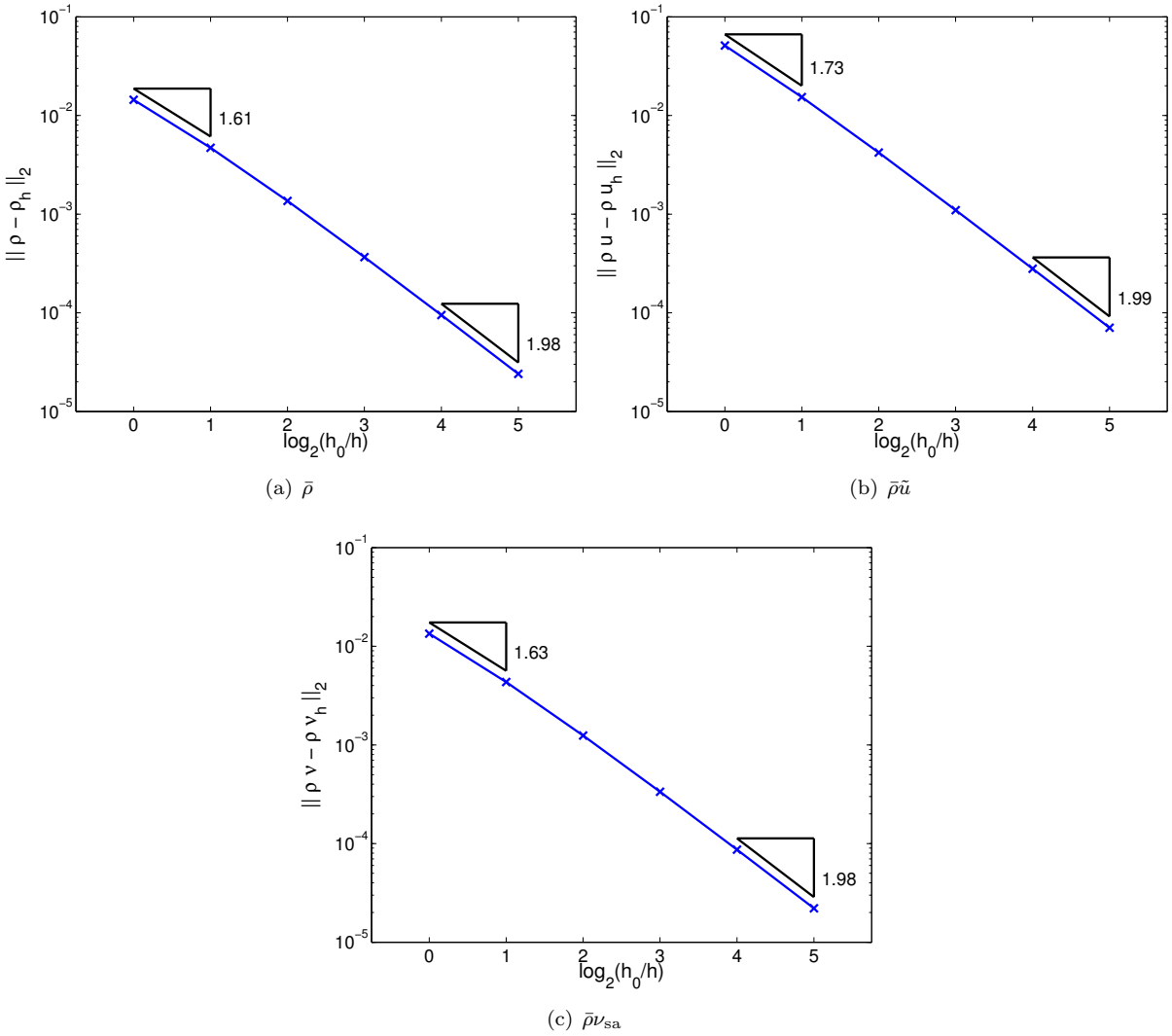

(a) $\bar{\rho}$ (b) $\bar{\rho}\tilde{u}$

(c) $\bar{\rho}\nu_{\text{sa}}$

Figure 7. L_2 **error versus grid refinement for the low** Re**, sinusoidal-based manufactured solution case.**

VI.B.1. Low Re

For the low Re case, μ and p_0 are set as follows:

$$\mu = 0.1\frac{\text{kg}}{\text{ms}}, \quad p_0 = 100\frac{\text{N}}{\text{m}^2}.$$

All other parameters are set to their default values, as given in Appendix A.B. These parameters settings lead to a very low Re case that exercises the SUPG discretization in the diffusion-dominated regime.

A mesh refinement study over a sequence of 11 uniform, anisotropic meshes has been performed. The coarse mesh is 16×16 elements. Each subsequent mesh is refined by a factor of approximately $\sqrt{2}$ in both directions, leading to a fine mesh of 512×512 elements. Figure 9 shows the resulting error, measured in the L_2 norm, as a function of mesh refinement. The figure shows that the asymptotic convergence rate is $\mathcal{O}(h^2)$. As in the low Re sinusoidal case, on the initial coarse meshes, the suboptimal convergence is consistent with that expected for the SUPG scheme implemented in FIN-S in the transition between the convection and diffusion dominated limits.

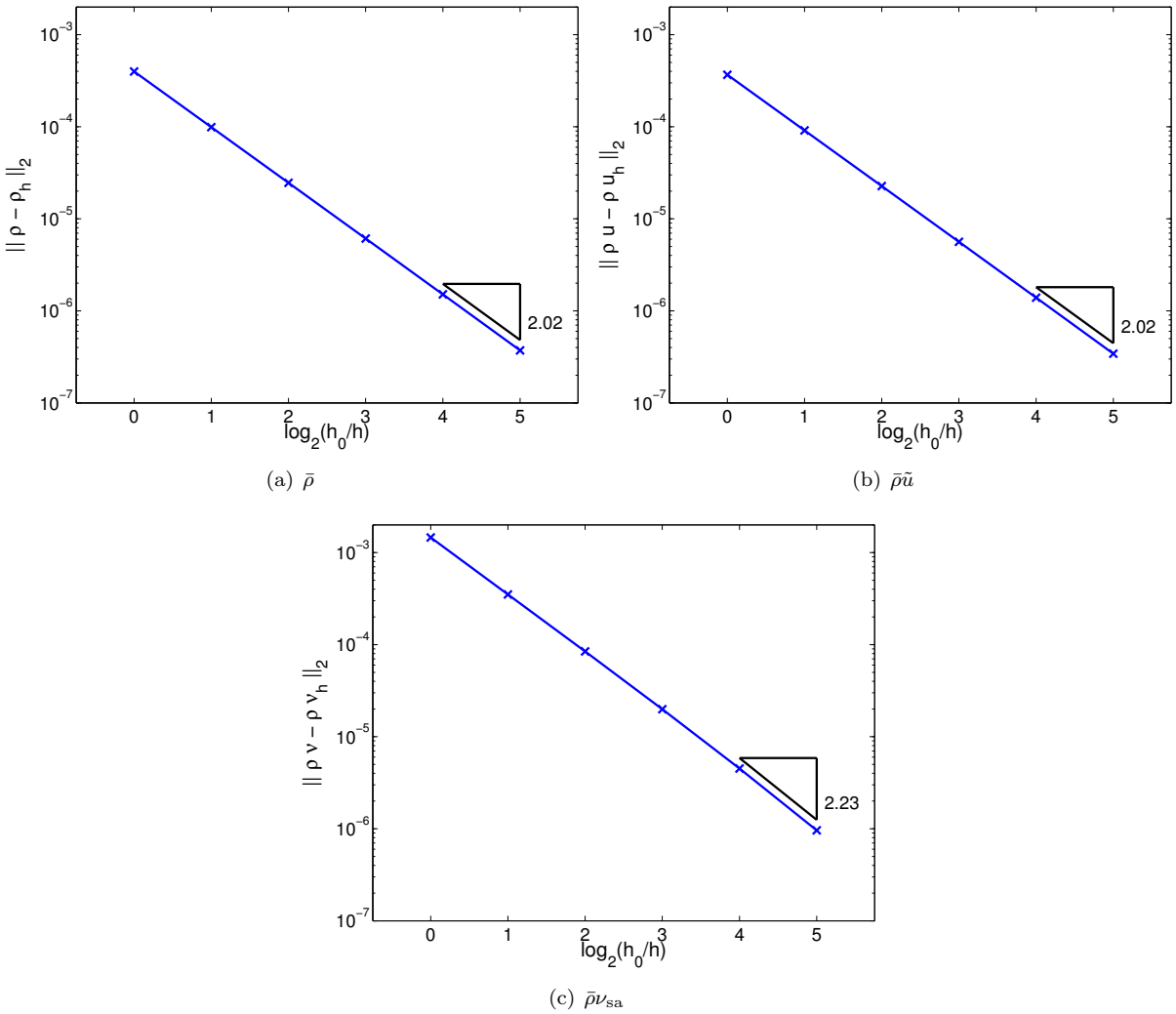

(a) $\bar{\rho}$ (b) $\bar{\rho}\tilde{u}$

(c) $\bar{\rho}\nu_{\text{sa}}$

Figure 8. L_2 error versus grid refinement for the high Re, sinusoidal-based manufactured solution case.

VI.B.2. High Re

For the high Re case, μ and p_0 are set as follows:

$$\mu = 1 \times 10^{-4} \frac{\text{kg}}{\text{ms}}, \quad p_0 = 1 \times 10^{4} \frac{\text{N}}{\text{m}^2}.$$

All other parameters are set to their default values, as given in Appendix A.B. These parameters settings lead to a high Re case. The Reynolds number based on the freestream conditions at $x = 1$ is $Re_x = 3.5 \times 10^5$. Furthermore, because the speed of sound is large, even near the wall, the Reynolds number based on mesh spacing and the speed of sound is larger than one. Thus, even near the wall, this case exercises the SUPG scheme in the convection-dominated regime. Of the four shown here, this case is the most physically realistic, and it is the closest to the actual use scenario of most turbulent FIN-S simulations.

A mesh refinement study was conducted over a sequence of 12 uniform, anisotropic meshes. To achieve reasonable resolution in y, the coarse mesh has 4×32 elements. Each subsequent mesh is refined by a factor of approximately $\sqrt{2}$ in both directions, leading to a fine mesh of 181×1448 elements. Figure 10 shows the resulting error, measured in the L_2 norm, as a function of mesh refinement. While there is some inconsistency in the order on the coarse meshes, on the finer meshes, the expected $\mathcal{O}(h^2)$ behavior is observed.

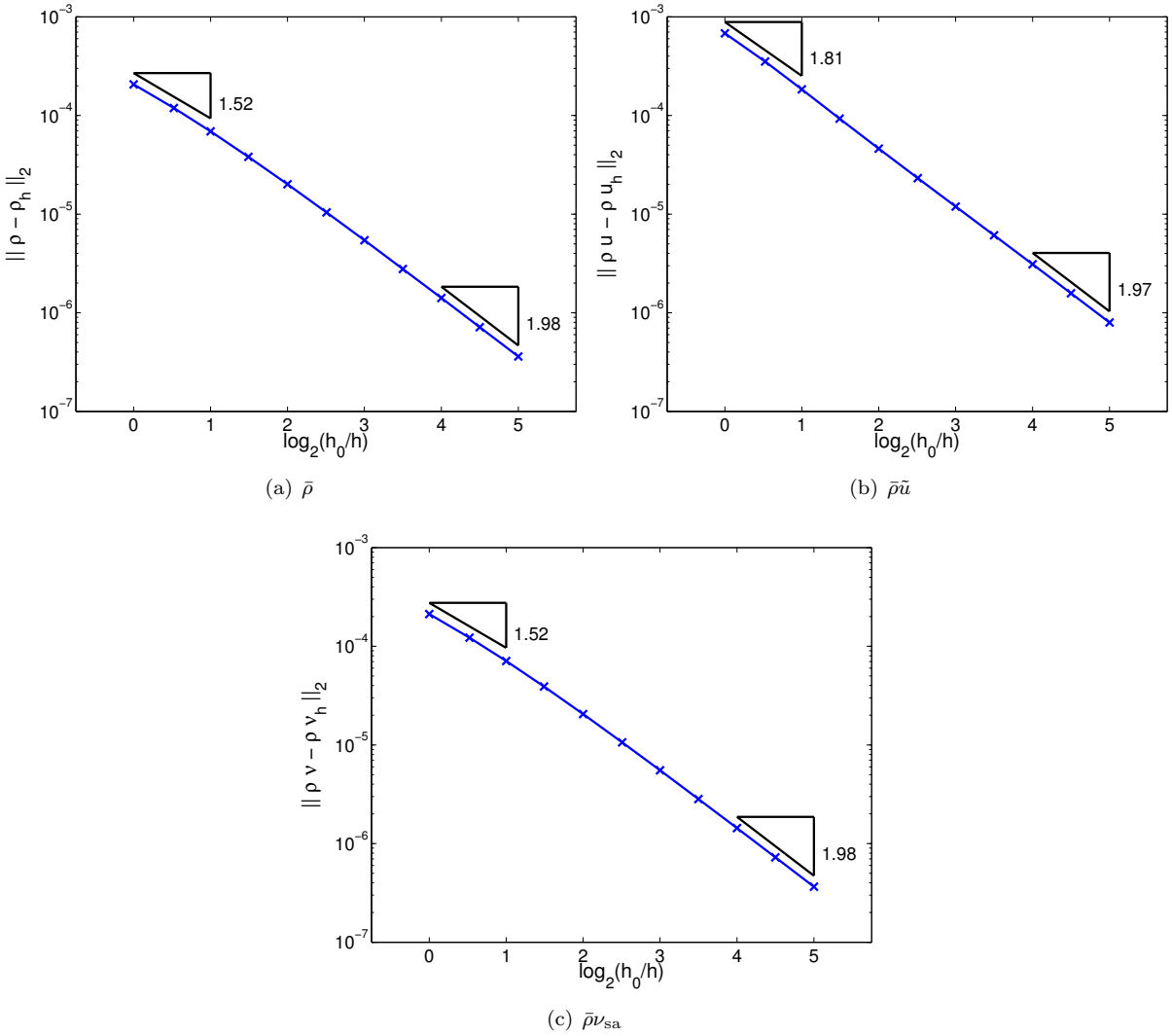

Figure 9. L_2 **error versus grid refinement for the low** Re**, physically-based manufactured solution case.**

VII. Conclusions

The MMS is a powerful technique for verification. In this work, the MMS was applied to verify the implementation of the FANS-SA equations in the FIN-S flow solver. The primary contribution of the work is a new manufactured solution for wall-bounded turbulent flow with the SA model. Previously proposed manufactured solutions for this case were analyzed and shown not to replicate desired features of the SA solution near the wall. This failure can lead to verification failures that are unrelated to the numerical implementation being tested. These problems are overcome here by developing a manufactured solution using well-known correlations from the turbulent boundary layer literature as well as the expected near-wall behavior of the SA solution. The resulting manufactured velocity profile has the expected qualitative features of an actual turbulent velocity profile for wall-bounded flow. Furthermore, when evaluated using the manufactured solution, all terms of the SA model have the correct near-wall asymptotic behavior. Grid convergence studies show that the FIN-S implementation of the SA model gives the expected second-order accuracy for both wall-bounded and unbounded flows in both the convection- and diffusion-dominated limits of the SUPG scheme.

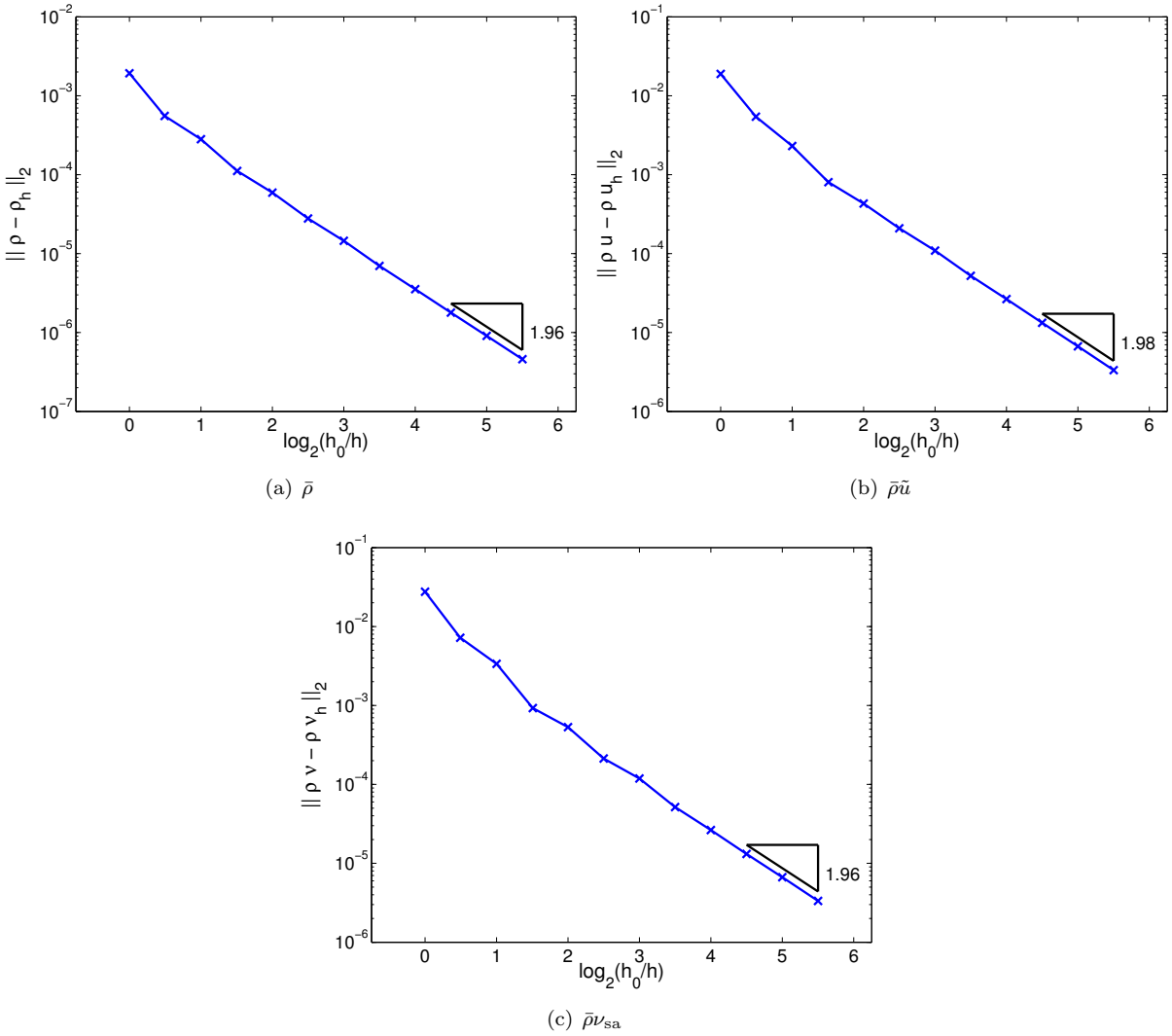

Figure 10. L_2 error versus grid refinement for the high Re, physically-based manufactured solution case.

A. Parameters and Constants

A.A. Sinusoidal-based Manufactured Solution

Table 1 summarizes the parameters of the sinusoidal-based manufactured solution presented in Section IV.A, recalling that in Equation (IV.A), $(\cdot) = \rho$, u, v, p or ν_{sa}, and $L = 1.0$. The $(\cdot)$ parameters have the same units as the variables. Thus, ρ_0, ρ_x, ρ_y are given in kg/m^3, u_0, u_x, u_y, v_0, v_x, v_y are given in m/s, p_0, p_x, p_y are given in N/m^2 and $\nu_{\text{sa}0}$, $\nu_{\text{sa}x}$, $\nu_{\text{sa}y}$ are given in m^2/s. The parameters $a_{\cdot x}$ and $a_{\cdot y}$ are dimensionless constants.

A.B. Physically-based Manufactured Solution

This section summarizes the parameters of the physically-based manufactured solution described in Section IV.B. Table 2 details the parameters of the manufactured solution. Table 3 presents the parameters required to specify the source term required by the MMS.

Finally, there are a number of additional constants that appear in the solution and that can be computed from the parameters. These constants should not be user-specified parameters and are listed in Table 4.

Table 1. Parameters required to specify the sinusoidal-based manufactured solution. $(\cdot) = \rho,\ u,\ v,\ p$ or ν_{sa} and L=1.0.

Equation/Parameter	$(\cdot)_0$	$(\cdot)_x$	$(\cdot)_y$	$a_{\cdot x}$	$a_{\cdot y}$
$\bar{\rho}$	1.0	0.1	-0.2	1.0	1.0
$\tilde{u}$	10.0	1.0	8.0	3.0	1.0
$\tilde{v}$	0.0	0.0	1.0	2.0	0.5
$\bar{p}$	1.0×10^5	10.0	10.0	2.0	1.0
ν_{sa}	0.2	0.1	0.2	0.5	1.0

Table 2. Parameters required to specify the physically realistic manufactured solution.

Parameter	Nom. Val.	Units	Explanation
C_{cf}	0.027	–	Incompressible skin friction fit parameter.
κ	0.41	–	von Karman constant.
η_1	11.0	–	Incompressible velocity profile model.
b	0.33	–	Incompressible velocity profile model.
C	5.0	–	Incompressible velocity profile model.
η_v	30.0	–	Wall normal velocity parameter.
T_∞	250.0	K	Freestream temperature.
M_∞	0.8	–	Freestream Mach number.
r_T	0.9	–	Recovery factor.
γ	1.4	–	Ratio of specific heats $= c_p/c_v$.
p_0	1e4	N/m^2	Mean pressure (constant throughout domain).
R	287.0	J/(kg K)	Gas constant $= c_p - c_v$.
α	5.0	1/s	Eddy viscosity quadratic term parameter.

Table 3. Additional parameters required to specify source term for the physically realistic manufactured solution.

Parameter	Nom. Val.	Units	Explanation
μ	1e-4	kg/(m s)	Fluid dynamic viscosity (constant throughout domain).
Pr	0.71	–	Prandtl number.
Pr_t	0.9	–	Turbulent Prandtl number.
c_{b1}	0.1355	–	SA model parameter.
σ_{sa}	2.0/3.0	–	SA model parameter.
c_{b2}	0.622	–	SA model parameter.
c_{w2}	0.3	–	SA model parameter.
c_{w3}	2.0	–	SA model parameter.
c_{v1}	7.1	–	SA model parameter.
c_{v2}	0.7	–	SA model parameter.
c_{v3}	0.9	–	SA model parameter.

Table 4. Constants that can be computed from the parameters of the physically realistic manufactured solution.

Constant	Expression	Explanation
u_∞	$M_\infty\sqrt{\gamma R T_\infty}$	Freestream velocity.
ρ_w	$p_0/(RT_w)$	Density at the wall.
F_c	$(T_w/T_\infty - 1)/(\sin^{-1} A)^2$	Skin friction transformation parameter.
T_w	$T_\infty\left[1 + r_T\frac{\gamma-1}{2}M_\infty^2\right]$	Wall temperature.
ρ_∞	$p_0/(RT_\infty)$	Freestream density.
ν_w	μ/ρ_w	Kinematic viscosity at the wall.
A	$\sqrt{1 - T_\infty/T_w}$	Constant in van Driest transform.
c_p	$(\gamma R)/(\gamma - 1)$	Specific heat at constant pressure.
c_v	$R/(\gamma - 1)$	Specific heat at constant volume.
c_{w1}	$c_{b1}/\kappa^2 + (1 + c_{b2})/\sigma_{\text{sa}}$	SA equation constant.

Acknowledgments

This material is based in part upon work supported by the Department of Energy [National Nuclear Security Administration] under Award Number [DE-FC52-08NA28615].

References

[1]AIAA Computational Fluid Dynamics Committe on Standards, "Guide for Verification and Validation of Computational Fluid Dynamics Simulations," AIAA G-077-1998, 1998.

[2]Roache, P. J., *Verification and Validation in Computational Science and Engineering*, Hermosa Publishers, 1998.

[3]American Society of Mechanical Engineers, "Guide for Verification and Validation in Computational Solid Mechanics," ASME V&V 10 2006, 2006.

[4]Oberkampf, W. L. and Roy, C. J., *Verification and Validation in Scientific Computing*, Cambridge University Press, October 2010.

[5]Roache, P. J. and Steinberg, S., "Symbolic Manipulation and Computational Fluid-Dynamics," *AIAA Journal*, Vol. 22, No. 10, 1984, pp. 1390–1394.

[6]Steinberg, S. and Roache, P. J., "Symbolic Manipulation and Computational Fluid Dynamics," *Journal of Computational Physics*, Vol. 57, No. 2, 1985, pp. 251–284.

[7]Spalart, P. R. and Allmaras, S. A., "A One-Equation Turbulence Model for Aerodynamic Flows," *La Recherche Aerospatiale*, Vol. 1, 1994, pp. 5–21, See also AIAA Paper 1992-439.

[8]Kirk, B. S. and Carey, G. F., "Development and Validation of a SUPG Finite Element Scheme for the Compressible Navier-Stokes Equations using a Modified Inviscid Flux," *Int. J. Numer. Meth. Fluid.*, Vol. 57, No. 3, 2008, pp. 265–293.

[9]Kirk, B. S. and Carey, G. F., "Validation of Fully Implicit, Parallel Finite Element Simulations of Laminar Hypersonic Flows," *AIAA J.*, Vol. 48, No. 6, 2010, pp. 1025–1036.

[10]Roy, C. J., Tendean, E., Veluri, S. P., Rifki, R., Hebert, S., and Luke, E. A., "Verification of RANS Turbulence Models in Loci-CHEM Using the Method of Manufactured Solutions," *18th AIAA Computational Fluid Dynamics Conference*, No. AIAA 2007-4203, 2007.

[11]Bond, R. B., Ober, C. C., Knupp, P. M., and Bova, S. W., "Manufactured Solution for Computational Fluid Dynamics Boundary Condition Verification," *AIAA Journal*, Vol. 45, No. 9, 2007, pp. 2224–2236.

[12]Eça, L., Hoekstra, M., Hay, A., and Pelletier, D., "Verification of RANS Solvers with Manufactured Solutions," *Engineering With Computers*, Vol. 23, No. 4, 2007, pp. 253–270.

[13]Eça, L., Hoekstra, M., Hay, A., and Pelletier, D., "A Manufactured Solution for a Two-Dimensional Steady Wall-Bounded Incompressible Turbulent Flow," *International Journal of Computational Fluid Dynamics*, Vol. 21, No. 3-4, 2007, pp. 175–188.

[14]Eça, L., Hoekstra, M., Hay, A., and Pelletier, D., "On the construction of manufactured solutions for one and two-equation eddy-viscosity models," *International Journal for Numerical Methods in Fluids*, Vol. 54, No. 2, 2007, pp. 119–154.

[15]Roy, C. J., Smith, T. M., and Ober, C. C., "Verification of a Compressible CFD Code using the Method of Manufactured Solutions," *32nd AIAA Fluid Dynamics Conference and Exhibit*, No. AIAA 2002-3110, 2002.

[16]Malaya, N., Estacio-Hiroms, K. C., Stogner, R. H., Schulz, K. W., Bauman, P. T., and Carey, G. F., "MASA: A Library for Verification Using Manufactured and Analytical Solutions," Manuscript submitted for publication to Engineering with Computers.

[17]Allmaras, S. R., Personal Communication via email with T. Oliver, Aug. 2007.

[18]Oliver, T. A. and Darmofal, D. L., "Impact of Turbulence Model Irregularity on High-Order Discretizations," *AIAA Paper 2009-953*, 2009.

[19]Hoekstra, M. and Eça, L., "PARNASSOS: An Efficient Method for Ship Stern Flow Calculation," *Osaka Colloquium*.

[20]Van Driest, E. R., "Problem of Aerodynamic Heating," *Aeron. Eng. Rev.*, Vol. 15, No. 10, October 1956, pp. 26–41.

[21]White, F. M., *Viscous Fluid Flow*, McGraw-Hill, 2nd ed., 1991.

[22]Spalding, D. B. and Chi, S. W., "The Drag of a Compressible Turbulent Boundary Layer on a Smooth Flat Plate with and without Heat Transfer," *J. Fluid Mech.*, Vol. 18, 1964, pp. 117–143.

[23]Cebeci, T., Chang, K., and Bradshaw, P., "Solution Of A Hyperbolic System Of Turbulence-Model Equations By The Box Scheme," *Computer Methods In Applied Mechanics And Engineering*, Vol. 22, No. 2, 1980, pp. 213–227.

[24]Kirk, B. S., Peterson, J. W., Stogner, R. H., and Carey, G. F., "`libMesh`: A C++ Library for Parallel Adaptive Mesh Refinement/Coarsening Simulations," *Engineering with Computers*, Vol. 22, No. 3–4, 2006, pp. 237–254.